



A sustainable exergy model for energy–water nexus in the hot regions: integrated combined heat, power and water desalination systems

Mehran Ansari¹ · Armin Beitollahi¹ · Pouria Ahmadi¹ · Behnaz Rezaie²

Received: 14 May 2020 / Accepted: 20 June 2020 / Published online: 24 July 2020
© Akadémiai Kiadó, Budapest, Hungary 2020

Abstract

Water scarcity is a worldwide concern for Earth citizens. Finding new methods for water concentration is essential for the extension of life. The water issue is more intense in the regions with a warm to the tropical environment. Considering the cooling demand of these regions, which consequently requires excess energy to satisfy the cooling load, having a thermal system to support three concerns of the water, cooling, and power would be the key for the warm/hot weather areas. In the present study, a novel model by integration of gas turbine power cycle with a solar parabolic collector, a steam turbine, heat recovery, steam generator, multi-effect desalination, and absorption chiller is proposed. The suggested model is optimized through developing a comprehensive multi-objective function to maximize the exergy efficiency and minimize the cost. Using the genetic algorithm method, the model is optimized based on six design parameters such as condenser pressure, number of solar parabolic through collector rows, gas turbine and steam turbine inlet temperature, high and low pressure, high- and low-pressure pinch points. The final optimal design point of this cycle enables the overall exergy efficiency of 36.16% and 188.43 \$ h⁻¹ of the total cost rate value; also, this integrated energy system provides the net electrical generation of 5.18 MW and the cooling load rate of 406.18 KW and generates 2.57 kg s⁻¹ of desalinated water. In this novel cycle solar energy is used for preheating the inflow of the combustion chamber. A dual pressure heat recovery exploits thermal energy of flue gas, which runs both desalination and multi-effect absorption system and circulates in simultaneous water and cooling load generation. Finally, by utilizing the genetic 1 algorithm, the optimal system is developed.

Keywords Integrated combined power plant · Gas turbine · Heat recovery · Absorption chiller · Genetic algorithm optimization · Double-effect desalination

List of symbols

P	Pressure
T	Temperature
Pr	Pressure ratio
η	Efficiency
h	Enthalpy
\dot{W}	Power
\dot{m}	Mass flow rate
G_b	Solar irradiance

S	Useful energy gain
ρ_c	Specular reflectance
γ	Intercept factor
τ	Transmittance
α	Absorptivity
ε	Emissivity
σ	Stefan Boltzmann constant
K_r	Incidence angle modifier
A	Area
W	Width
L	Tube length
D	Diameter
R_u	Universal gas constant
CRF	Capital recovery factor
COP	Coefficient of performance
Nu	Nusselt number
K	Thermal conductivity
Q	Heat transfer
Re	Reynolds number
U	Thermal conductance

✉ Pouria Ahmadi
Pahmadi@ut.ac.ir

✉ Behnaz Rezaie
Rezaie@uidaho.edu

¹ School of Mechanical Engineering, College of Engineering, University of Tehran, P.O. Box 11155-4563, Tehran, Iran

² Applied Energy Research Laboratory (AERL), Department of Mechanical Engineering, College of Engineering, University of Idaho, 875 Perimeter Dr, Moscow, ID 83844-0902, USA

Pr	Prandtl number
Es	Sun exergy
LHV	Lower heating value
HP	High pressure
LP	Low pressure
pcf	Pressure correction factor
tcf	Temperature correction factor
ER	Entrainment ratio
CR	Compression ratio
X	Salinity
<i>M</i>	Molar mass
<i>C</i>	Concentration
$\dot{E}X$	Total exergy
ex	Specific exergy
cost	Cost
c_{fuel}	Fuel cost

Subscript

comp	Compressor
a	Absorber
r	Receiver
c	Collector
∞	Free stream
s	Sun
cc	Combustion chamber
g	Flue gas
cond	Condenser
eva	Evaporator
abs	Absorber
gen	Generator
ST	Steam turbine
ch	Chemical
ph	Physical
GT	Gas turbine

Introduction

The increase in population results in inevitable bulged demands for energy and water. Though finding approaches for satisfying the growing demands is drawing much attention, one of the efficient approaches is using district energy systems (DES) for populated areas since there are controls on energy resources, generations, storage, and distributions to consumers by energy plants' management and their high efficiency and environmental friendliness [1, 2]. One of the favorable energy system models for the DES is integrating steam turbine with a gas turbine combined cycle power plants (CCPPs) [3]. The important parameters in the designing of a DES are environmental impacts, energy resources, costs, and energy efficiency [4]. Energy efficiency improvement is achievable by several methods like exergy analysis, parametric study, and optimization of a

cycle [5]. Integrating renewable energy with DES improves energy sustainability and reduces environmental impacts [6]. Thermal solar panels could be considered as alternatives for preheating the vapor or gas turbine working fluids [7]. Also, solar panels have shown a significant effect on heat pump efficiency on both cooling and heating modes [8]. Mokhtari et al. used a comprehensive solar collector system to preheat the process fluid of furnace in a refinery in a case study and decreased about 24% of the furnace consumption [9]. Arabkoohsar and Sadi used a coupled waste-solar steam generator in a power plant [10]. The thermal efficiency of their cycle was around 25% which was suitable for a cycle with solar concentrating units. In another study Acar and Arslan investigated a coupled solar and geothermal organic Rankine cycle (ORC) and achieved an exergy efficiency of 64% [11]. Water is one of the most important essential for life. It is predicted that population and consequently water demand increase, while climate change negatively greater impacts natural water sources by 2050 [12]. People in most parts of the world including the Middle East are facing water challenges where food, energy, and water security are mainly affected by drought, water scarcity, population growth, urbanization, and/or political unrest [13]. Near 97% of the Earth's water are oceans that are not suitable to satisfy human needs with such a sharp population and demand increase. For that reason, many energy studies are integrated with water desalination to generate drinkable water from seawater [14]. Water treatments are including membrane, and evaporation-based technology, evaporative-based desalination, consumes lower initial cost and could be easily scaled up; also it can be integrated to heat recovery energy system [15]. Membrane-based desalination has low working energy but high maintenance cost [16]. Multi-effect desalination can be integrated with the energy cycle. Farsi and Dincer investigated a combination of water-ground hot steam, steam turbine, desalination, and PEM and showed that the system was capable of producing more than 165,600 kg of drinkable water per day [17]. Also, Vakilabadi et al. suggested zero liquid discharge for treating brine of power plant and investigated effects of the dimensional and operating parameters on the freshwater, efficiency, and the total power consumption [18]. Rostamzade et al. integrated absorption-compression heat pump with a vapor compression heat pump and a MED unit and then compared that with a conventional mechanical vapor compression MED unit. They showed the integrated units had higher exergy efficiency [19]. Aguilar-Jiménez et al. combined ORC with a MED unit and concluded that the MED/ORC integration benefits both final production of pure water and efficiency [20]. Combination of different systems including gas turbine, steam turbine, absorption chiller, the solar panel has been investigated in several studies. Mahdavi and Khalilarya combined a gas turbine

heat recovery steam generator (HRSG)/ORC cogeneration system with a parabolic trough solar collectors field and concluded the combined system had higher performance than the initial system [21]. Huang et al. enhanced primary energy saving rate and reduced the CO₂ emission rate by investigating the energy distribution and exergy destruction of a CCHP system under different gas turbine loads and rate. Wang et al. used the waste heat of a GT with a solar system in a double effect LiBr absorption chiller [22]. They found that compared to the system without solar energy, the proposed hybrid system's carbon emission reduction ratio is approximately 41%. Lake et al. found the right percentage of LiBr concentration in the absorption chiller by using exergy analysis [6]. They conclude the higher concentration altered the internal temperatures by 3 °C–7 °C, while the lower concentration led to an increase in the exergy destruction rates. Naseri et al. introduced a novel CO₂ transcritical power cycle combined with solar energy integrated by the cryogenic LNG recovery unit to improve the total owed of the cycle in the off-peak times and peak time [23]. In their investigation, the solar system has a prominent effect on cycle performance. Also, a recent study show using gas turbine in several industries with hot gases can reduced pollution. Jalili et al. used a gas turbine with a heat recovery system after a cement industry [24]. The present study

investigates a novel DES model which combines several systems to supply electrical energy and water demands of consumers in a hot environment exergetically and economically. The model consists of a solar thermal panel, gas turbine, HRSG, steam turbine, MED desalination, and a double-effect absorption chiller. The exergy efficiency and cost rate of the proposed model will be optimized for each cycle using the genetic algorithm method for higher performance based on the design parameters which will be developed through the sensitivity test.

Proposed integrated energy system model

The proposed CHP and water desalination plant is shown in Fig. 1. The cycle consists of five primary parts: gas turbine plant, steam turbine plant, HRSG, MED, and a double-effect absorption chiller. With a thermodynamic view, the proposed plant consists of four cycles as the solar Bryton cycle, HRSG, MED, and a double-effect absorption chiller. In Fig. 1, C# and D# represent absorption chiller and desalination system stages, respectively.

Air at ambient pressure and temperature enters the compressor in the solar Bryton cycle. The SPTC system preheats the compressed air before entering the combustion chamber (CC). Combustion of heated compressed

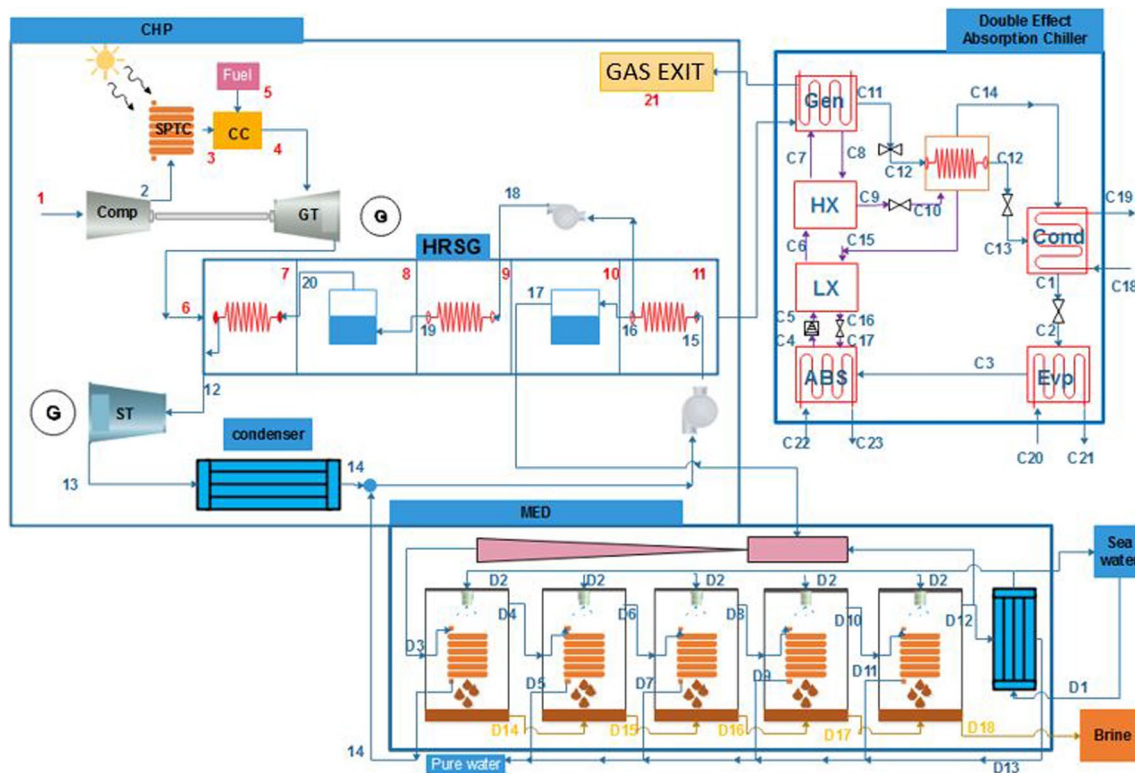


Fig. 1 The schematic of the proposed integrated energy system for CHP and water desalination. In this figure, D and C stand for desalination and chiller, respectively. Numbers illustrated in the figure represent distinctive thermodynamic states as reported in tables of section “Data”

air with methane (CH₄) at standard conditions results in hot gases, which generates electrical power through the turbine. The HRSG generates vapor by the expanded hot gases for both steam turbine to generate electricity and multi-effect desalination to purify the water.

The HRSG system consists of five effects such as high-pressure super heater, high-pressure vapor drum, high-pressure economizer, low-pressure drum, and a total flow economizer. The high-pressure line is superheated to enter the steam turbine, and low-pressure line is saturated to enter the MED system. Saturated water of two different lines discharging from the steam turbine and MED systems is mixed to enter low-pressure pump. After heating the water in the total flow economizer, this line splits into two lines; one enters the low pressure drum to generate the saturated vapor in low-pressure condition to enter the MED system, and the other enters the high-pressure economizer to reach the saturated liquid condition. Saturated liquid enters high-pressure drum and converts to high-pressure saturated vapor to become superheated in the high-pressure superheater, which is the last effect of HRSG.

The absorption chiller is a double-effect LiBr-H₂O type, which includes high- and low-pressure generators, an evaporator, a condenser, an absorber, a high-temperature heat exchanger, a low-temperature heat exchanger, two pressure reducing valves, two refrigerant expansion valves, and a refrigerant valve with switches to control. In heating mode, the absorption chiller is like a heat exchanger, and there is no refrigerant effect in its cycle. Also, there are two heat exchangers to preheat the weak solution line with a strong solution one.

The last component of the integrated system, the MED system, is a five-effect desalination system, including an ejector that drops the pressure of the saturated vapor and returns the saturated water to the cycle. Finally, using the genetic algorithm, the proposed cycle is optimized.

Methodology

The approach in this study is a thorough parametric study; the effectiveness of each input parameter on exergy efficiency and total cost rate of the whole system is investigated. Then, most effective parameters are used in the optimization of the system. To do so, all physical and financial relationships for different components need to be developed in detail first. Here, step-by-step required equations for various components are developed either based on the universal laws or referencing previous studies.

Exergy

Exergy analysis is a tool for measuring the useful energy. There are two noticeable types of exergy in this study: physical and chemical. Physical exergy is achieved as the system reaches ambient temperature with no change of its composition, while the chemical exergy is related to change in the composition.

Physical exergy

Physical exergy of each state is defined as:

$$ex_{ph} = (h - h_0) - T_0(s - s_0) \quad (1)$$

$$\dot{E}X_{ph} = \dot{m}ex_{ph} \quad (2)$$

Chemical exergy

In the integrated cycle of this study, there are three states where chemical exergy needs to be considered: combustion chamber, absorption chiller, and MED. The following equations are used for all these three subsystems to obtain their chemical exergy. The standard chemical exergy of each component according to the conforming partial pressure P_i with respect to the ambient pressure P_0 and the ambient temperature T_0 is defined as:

$$\overline{ex}_{ch}^i = RT_0 \ln \left(\frac{P_0}{P_i} \right) \quad (3)$$

Having a mixture of components, the overall specific chemical exergy according to the molar fraction x_i and the consideration of the standard exergy is written as:

$$ex_{ch} = \sum_{i=1}^n x_i \overline{ex}_{ch}^i + RT_0 \sum_{i=1}^n x_i \ln(x_i) \quad (4)$$

Finally, the overall exergy rate is available by multiplying the molar flow rate to the overall specific chemical exergy as:

$$\dot{E}X_{ch} = \dot{N}ex_{ch} \quad (5)$$

For the case of MED, as the variation of salt concentration applies to the sea water, sea water state must be considered as the reference situation (reference concentration) in order to calculate the chemical exergy. Finally, the total exergy is defined as the summation of chemical and physical exergy.

$$\dot{E}X_{total} = \dot{E}X_{ph} + \dot{E}X_{ch} \quad (6)$$

Overall cycle exergy efficiency

Overall exergy efficiency represents the ratio of useful recovered exergy to the useful available exergy of a system, which is a representative of system’s performance of how efficiently a system delivers work according to its available energy in the form of useful work. Here, in this study, the overall cycle exergy efficiency is considered as the ratio of the useful obtained exergy which is the summation of net electrical generated power, desalination and chiller systems’ net total exergy to the input exergy acquired from solar collectors and fuel.

$$\eta_{ex} = \frac{\dot{W}_{net} + \dot{E}X_{desalination} + \dot{E}X_{chiller}}{\dot{E}X_{sun} + \dot{E}X_{fuel}} \tag{7}$$

Here, subscripts desalination, chiller, sun, and fuel represent the exergy associated with freshwater production, cooling production, the exergy of sun, and exergy of fuel. More details about each term are given in [25].

Coefficient of performance (COP)

COP is defined as the ratio of desired output to the required input in the form of heat transfer. In the case of the absorption chiller, the desired output heat is the cooling load extracted by the evaporator, and the required input heat is the heat energy applied to the generator of the chiller. Therefore, with respect to the mentioned concepts, the overall energy balance of the absorption chiller neglecting the pumps input energy yields:

$$\dot{Q}_{gen} + \dot{Q}_{eva} = \dot{Q}_{abs} + \dot{Q}_{cond} \tag{8}$$

And finally, coefficient of performance of absorption chiller is defined as:

$$COP = \frac{\dot{Q}_{eva}}{\dot{Q}_{gen}} \tag{9}$$

Economic analysis

Economic analysis consists of initial cost of each component and total cost rate of cycle.

Initial cost

Each of the equipment of cycle can be financially valued by its physical parameters. Every single equipment has a

prominent design parameter that defines its cost as it is provided in section “Initial cost”.

Total cost rate

Initial costs are transformed to cost rate by considering the following assumptions [26]

- 20 years of operations as each devices life time (n)
- 7200 hours of function within each year (N)
- 6% addition to the initial costs with purpose of operation and maintenance (φ)
- A fixed base price of 0.003 \$ MJ⁻¹ for fuel cost (c_{fuel})

According to the assumptions above, the capital recovery factor (CRF) is obtained as:

$$CRF = i \times \frac{(1 + i)^n}{(1 + i)^n - 1} \tag{10}$$

By multiplying this parameter to the initial cost, one can find the initial cost rate in (\$ h⁻¹) unit. In addition, cost rate of fuel is calculated as a function of fuel unit cost (C_{fuel}), the lower heating of fuel (LHV) as the H₂O in combustion products is in gas form, we use LHV and the fuel mass flow rate as [26]:

$$\text{fuel cost rate (\$ h}^{-1}\text{)} = \dot{m}_{fuel} \times c_{fuel} \times \frac{LHV}{10^6} \times 3600 \tag{11}$$

By summation of these cost rates, we reach the total cost rate of cycle in dollars per hour as:

$$\text{Total cost rate (\$ h}^{-1}\text{)} = \frac{CRF\varphi}{N} \sum \text{initial cost rates} + \text{fuel cost rate} \tag{12}$$

Brine enthalpy

The first law analysis of the MED system requires the enthalpy of each stream being known, which necessitates a suitable model providing the enthalpy of brine solution. Here, a model for brine enthalpy is employed as [16]

$$h_0 = 9.6296X - 0.4312402 \times 10^{-3}X^2 \tag{13}$$

$$A = 4206.8 - 6.6197X + 0.012288X^2 \tag{14}$$

$$B = -1.1262 + 0.054178X - 2.2719 \times 10^{-4}X^2 \tag{15}$$

$$C = 0.012026 - 5.3566 \times 10^{-4}X + 1.8906 \times 10^{-6}X^2 \tag{16}$$

$$D = 6.8777 \times 10^{-7} + 1.517 \times 10^{-6}X - 4.4268 \times 10^{-9}X^2 \tag{17}$$

$$h = h_0 + A(T - 273.15) + \frac{B}{2}(T - 273.15)^2 + \frac{C}{3}(T - 273.15)^3 + \frac{D}{4}(T - 273.15)^4 \quad (18)$$

where h represents the enthalpy of brine with respect to its concentration.

Analysis

In this section, thermodynamic analysis, including the first law of thermodynamics and exergy analysis, is carried out in detail for the cycle's subsystems. As explained in "Proposed integrated energy system model" section, the cycle is categorized into four parts: a solar Brayton cycle, a heat recovery steam generator (HRSG), a multi-effect desalination (MED) unit, and a double-effect absorption chiller. In the following, details are presented.

Solar Bryton cycle

Solar Brayton cycle, as mentioned before, includes an air compressor, solar parabolic through collectors, a combustion chamber, and a gas turbine. The following thermodynamic relations are used for modeling of the cycle. For the simulation of this part, the inputs are applied to the computer simulation code developed in MATLAB software, and thermo-physical properties are acquired by calling the CoolProp library within the simulation code. Each component is developed in MATLAB Mfile for the sake of simplicity and easy to track. In the following sections, we explain the thermodynamic modeling.

Air compressor

Inlet air temperature, inlet air pressure, compressor's isentropic efficiency, and compressor pressure ratio are the input parameters in the gas turbine power plants. The outlet pressure, temperature, enthalpy, and work are the unknowns that should be determined. By having the inlet air conditions to the compressor and its pressure ratio, the outlet pressure can be written as

$$P_2 = P_1 \text{Pr}_{\text{comp}} \quad (19)$$

Now, according to the definition of isentropic efficiency, the outlet air enthalpy can be obtained as

$$h_2 = h_1 + \frac{(h_{2s} - h_1)}{\eta_{\text{comp}}} \quad (20)$$

where h_{2s} represents the isentropic discharge enthalpy of the compressor. Finally, the net required work of the compressor could be found by using first law of the thermodynamics on compressor as

$$\dot{W}_{\text{comp}} = \dot{m}_2(h_2 - h_1) \quad (21)$$

Solar parabolic through collector (SPTC)

SPTC consists of a solar parabolic collector and an intermediate-glass covered pipe at its focal point as shown in Fig. 2. Collection efficiency (η_r) and useful energy gain (S) based on solar radiation (G_b) are represented as [7]

$$\eta_r = \rho_c \gamma \tau \alpha K_r \quad (22)$$

$$S = G_b \eta_r \quad (23)$$

Here, ρ_c , γ , τ , α , and K_r show specular reflectance, intercept factor, transmittance, absorptivity, and incidence angle modifier, respectively, which are given in the table in section "Applied constants". Absorber (A_a) and receiver (A_r) areas are

$$A_r = \pi D_{ro} L \quad (24)$$

$$A_a = (W - D_{co}) L \quad (25)$$

Next, there is a set of equations to obtain the useful heat transferred to the inflow air and the rate of dissipated heat of the concentrator. The Nusselt number of the peripheral air is defined as below, and according to its definition, surrounding heat transfer coefficient can be obtained [7]

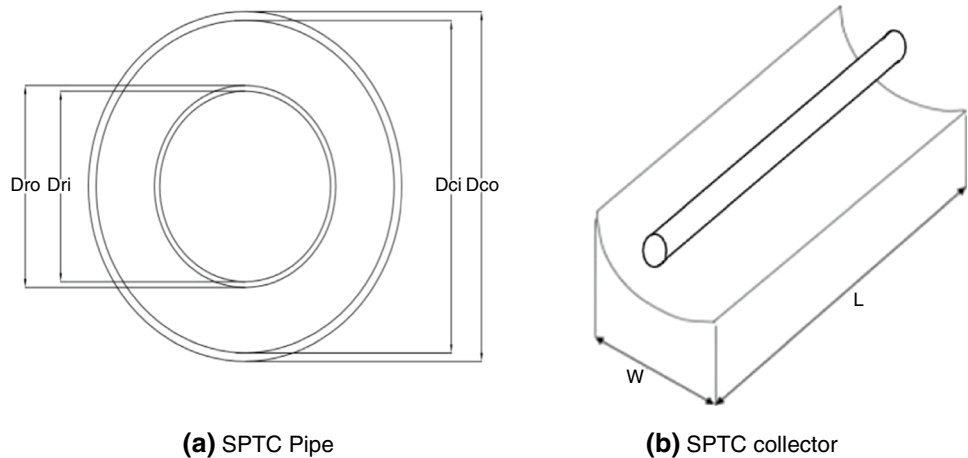
$$\text{Nu} = 0.3 \text{Re}^{0.6} \quad (26)$$

$$h_{\infty} = \frac{\text{Nu} \cdot K_{\infty}}{D_{co}} \quad (27)$$

Dissipated heat could be written in both forms of convection and radiation. The convection term accounts for heat transfer rate between the outer cover surface and its ambient one, and the radiation term is mainly the heat transfer rate between the outer cover surface and the sky; therefore, the term heat loss from the outer cover surface is written as

$$Q_{\text{loss}} = \pi D_{co} L h_{\infty} (T_{co} - T_{\infty}) + \epsilon_c \pi D_{co} L \sigma (T_{co}^4 - T_{\text{sky}}^4) \quad (28)$$

Fig. 2 Schematic of SPTC



And therefore, the overall heat transfer coefficient could be defined as

$$U_L = \frac{Q_{\text{loss}}}{A_r(T_r - T_\infty)} \tag{29}$$

Similarly, for the internal flow we have [7]:

$$\text{Nu}_f = 0.023\text{Re}_f^{0.8} \text{Pr}_f \tag{30}$$

$$h_f = \frac{\text{Nu}_f K_f}{D_{ri}} \tag{31}$$

The overall heat transfer coefficient between the ambient and inflow air based on the outside receiver diameter is written as

$$U_o = \left(\frac{1}{U_L} + \frac{D_{ro}}{D_{ri} h_f} + \frac{D_{ro}}{2K_{\text{tube}}} \ln \left(\frac{D_{ro}}{D_{ri}} \right) \right)^{-1} \tag{32}$$

And therefore, the collector efficiency factor F' is provided as

$$F' = \frac{U_o}{U_L} \tag{33}$$

Also the collector flow factor F'' is considered as

$$F'' = \frac{\dot{m}_f c p_f}{A_r U_L F'} \left(1 - \exp \left(\frac{-\dot{m}_f c p_f}{A_r U_L} \right) \right) \tag{34}$$

Having these two factors, ultimately the collector heat removal factor F_r is written as

$$F_r = F' F'' \tag{35}$$

The variable F_r is analogous to the effectiveness of a heat exchanger which is the ratio of the actual to the maximum possible heat transfer.

It is worth noting that the maximum possible rate of heat transfer among collectors could occur by being the entire collector temperature at the same temperature of the inlet flow since the rate of heat losses to the surrounding would be a minimum. Ultimately, multiplying the heat removal factor to the maximum possible rate of heat transfer yields the useful or actual rate of heat transferred to the internal airflow which is written as

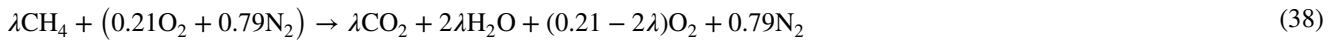
$$Q_u = F_r A_a \left(S - \frac{A_r}{A_a} U_L (T_r - T_\infty) \right) \tag{36}$$

And the collector’s exergy efficiency is modeled as [7]

$$Es = A_a G_b \left(1 - \frac{4}{3} \left(\frac{T_\infty}{T_s} \right) + \frac{1}{3} \left(\frac{T_\infty}{T_s} \right)^4 \right) \tag{37}$$

Combustion chamber (CC)

In this component, the hot air inlet conditions are defined, and the output temperature, which is called the turbine inlet temperature (TIT), is also defined. It is assumed that complete combustion with probable excess air occurs within the combustion chamber. Dominant chemical reactants with their conforming products are considered to form a chemical balance. However, the fuel-to-air ratio and the composition of flue gases should be calculated. Thus, by writing the chemical balance of the combustion process, it yields



By applying the mass continuum on CC, the following equation can be developed

$$\dot{m}_3 + \dot{m}_f = \dot{m}_g \quad (39)$$

Applying the first law of thermodynamics around the CC, it can be found that

$$\dot{m}_3 h_3 + \dot{m}_f \text{LHV} = \dot{m}_g h_4 \quad (40)$$

Also, there is pressure drop within the combustion the combustion chamber which could be modeled as

$$\frac{P_4}{P_3} = (1 - \Delta P_{cc}) \quad (41)$$

Here, ΔP_{cc} is the pressure drop coefficient across the combustion chamber provided in the table in section “Applied constants”. [26]. Thus, these equations are solved simultaneously, and fuel and air mass flow rate and flue gas compositions are calculated.

Gas turbine

Similar to the compressor, here, gas turbine inlet temperature (TIT), pressure ratio, and gas turbine isentropic efficiency are given, and outlet enthalpy, outlet pressure, and output power are to be calculated. Property calculation of the gas turbine is the same as the compressor; therefore, by reapplying the procedure, the electricity generation of the gas turbine would be obtained as [26].

$$P_4 = P_6 \text{Pr}_{\text{GT}} \quad (42)$$

Based on the energy efficiency definition of the turbine

$$h_6 = h_4 - \eta_{\text{turb}}(h_4 - h_6) \quad (43)$$

Applying the first law of the thermodynamics on the turbine results in [27]

$$\dot{W}_{\text{GT}} = \dot{m}_g(h_4 - h_6) \quad (44)$$

Heat recovery steam generator and steam turbine

For HRSG modeling, we have some inputs, and the outputs should be calculated. Of course, there are some design parameters, which are considered as input parameters. The most critical design parameters in each HRSG are pinch point temperatures, which are defined as the difference between the outlet temperature of the evaporator outlet gas

and the inlet water flow, and the HRSG pressure levels. In this case, the flue gas properties are considered as inputs as it was calculated from the gas turbine simulation. Flue gas temperature and compositions were already calculated in gas turbine modeling. Thus, the temperature of steam and gas along the HRSG should be calculated. Also, temperature variation along the HRSG is illustrated in Fig. 3. Applying the energy balance of the HRSG components, the thermodynamic properties of each state can be determined. They are provided as

$$\text{HP super heater} \quad \dot{m}_g(h_6 - h_7) = \dot{m}_{\text{HP}}(h_{12} - h_{20}) \quad (45)$$

$$\text{HP evaporator} \quad \dot{m}_g(h_7 - h_8) = \dot{m}_{\text{HP}}(h_{20} - h_{19}) \quad (46)$$

$$\text{HP economizer} \quad \dot{m}_g(h_8 - h_9) = \dot{m}_{\text{HP}}(h_{19} - h_{18}) \quad (47)$$

$$\text{LP evaporator} \quad \dot{m}_g(h_9 - h_{10}) = \dot{m}_{\text{LP}}(h_{17} - h_{16}) \quad (48)$$

$$\text{Economizer} \quad \dot{m}_g(h_{10} - h_{11}) = (\dot{m}_{\text{HP}} + \dot{m}_{\text{LP}})(h_{16} - h_{15}) \quad (49)$$

$$\dot{W}_{\text{ST}} = \dot{m}_{\text{HP}}(h_{12} - h_{13}) \quad (50)$$

Multi-effect desalination (MED)

MED system consists of an ejector; effects of desalination including five evaporators and a condenser are modeled as follows

Ejector

There are various models in order to correlate streams, and here a well-known semi-empirical model provided by El-Desouky [28] is considered. The entrainment ratio (ER) is defined as the ratio of the motive stream’s flow rate (state 17, the inlet to ejector from the HRSG) to the entrained vapor’s flow rate (state D12, the inlet to the ejector from the MED’s condenser). The compression ratio (CR) is defined as the ratio of the compressed vapor’s pressure (state D3, the outlet of the ejector) to the entrained vapor’s pressure (state D12, inlet to the ejector from the MED’s condenser). In order to obtain the entrainment ratio, two auxiliary parameters are defined. Motive stream pressure correction factor (pcf) and the entrained vapor temperature correction factor (tcf) are defined in Table 1. The

Fig. 3 Temperature variation along the HRSG

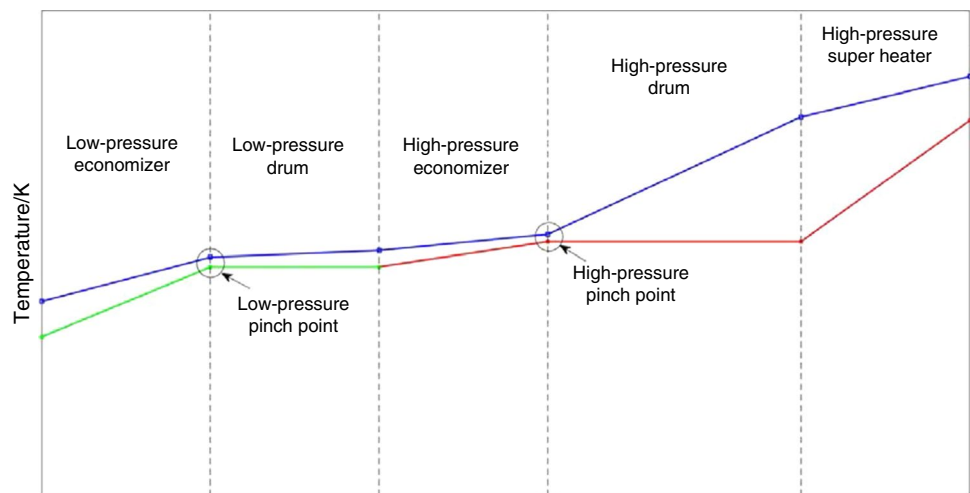


Table 1 Ejector’s performance parameters [28]

Parameter	Correlation
pcf	$3 \times 10^{-7} \left(\frac{P_{17}}{10^3}\right)^2 - 9 \times 10^{-4} \left(\frac{P_{17}}{10^3}\right) + 1.6101$ (51)
tcf	$2 \times 10^{-8} (T_{17} - 273.15)^2 - 6 \times 10^{-4} (T_{17} - 273.15) + 1.0047$ (52)
ER	$\frac{\dot{m}_{17}}{\dot{m}_{D12}}$ (53)
	$0.296 \left(\frac{P_{D3}}{10^5}\right)^{1.19} \left(\frac{P_{D12}}{10^3}\right)^{1.04} \left(\frac{P_{17}}{P_{D12}}\right)^{0.015} \left(\frac{pcf}{tcf}\right)$ (54)
CR	$\frac{P_{D3}}{P_{D12}}$ (55)

incorporation of these auxiliary parameters into Eq. (54) determines value of the entrainment ratio.

Note that the all input parameters of the above equations are in SI unit. There are several restrictions to this model as $10\text{ }^\circ\text{C} < T_{D12} < 500\text{ }^\circ\text{C}$, $100\text{ kPa} \leq P_{17} \leq 3500\text{ kPa}$, $CR > 1.81$, and $ER < 4$.

Effects of desalination

Several assumptions in modeling the MED system are made as in [16].

- Effects have the same feed sea water flow rate (\dot{m}_{D2})
- MED’s condenser temperature is 48 °C
- Temperature difference across the effects is the same
- A minimum temperature difference at the MED’s condenser is considered
- Final effect’s salinity is fixed (in the table in section “Data”)

Based on the given assumptions, it can be concluded that the temperature difference across the consecutive effects is [16]

$$\Delta T = \frac{T_{D14} - T_{D12}}{5} \tag{56}$$

And for the outlet temperature of effects, we have (here i represents the specific number of each effect plus one and therefore it is from 2 to 6)

$$T_{D(2i)} = T_{D3} - (i - 1)\Delta T \tag{57}$$

Finally, applying the first law, mass conservation, and concentration balance on all effects gives the following

First effect

$$\begin{aligned} \text{Energy conservation } & \dot{m}_{D3}h_{D3} + \dot{m}_{D2}h_{D2} \\ & = \dot{m}_{D4}h_{D4} + \dot{m}_{D14}h_{D14} + \dot{m}_{D3}h_{14} \end{aligned} \tag{58}$$

$$\text{Mass conservation } \dot{m}_{D2} = \dot{m}_{D4} + \dot{m}_{D14} \tag{59}$$

$$\text{Concentration balance } \dot{m}_{D2}X_{\text{sea}} = \dot{m}_{D14}X_{14} \tag{60}$$

Second effect

$$\begin{aligned} \text{Energy conservation } & \dot{m}_{D4}h_{D4} + \dot{m}_{D2}h_{D2} + \dot{m}_{D14}h_{D14} \\ & = \dot{m}_{D5}h_{D5} + \dot{m}_{D15}h_{D15} + \dot{m}_{D6}h_6 \end{aligned} \tag{61}$$

$$\text{Mass conservation } \dot{m}_{D2} + \dot{m}_{D14} = \dot{m}_{D6} + \dot{m}_{D15} \tag{62}$$

$$\text{Concentration balance } \dot{m}_{D2}X_{\text{sea}} + \dot{m}_{D14}X_{14} = \dot{m}_{D15}X_{15} \tag{63}$$

Third effect

$$\begin{aligned} \text{Energy conservation } & \dot{m}_{D6}h_{D6} + \dot{m}_{D2}h_{D2} + \dot{m}_{D15}h_{D15} \\ & = \dot{m}_{D7}h_{D7} + \dot{m}_{D16}h_{D16} + \dot{m}_{D8}h_8 \end{aligned} \tag{64}$$

$$\text{Mass conservation } \dot{m}_{D2} + \dot{m}_{D15} = \dot{m}_{D8} + \dot{m}_{D16} \tag{65}$$

$$\text{Concentration balance } \dot{m}_{D2}X_{\text{sea}} + \dot{m}_{D15}X_{15} = \dot{m}_{D16}X_{16} \tag{66}$$

Fourth effect

$$\begin{aligned} \text{Energy conservation } \dot{m}_{D8}h_{D8} + \dot{m}_{D2}h_{D2} + \dot{m}_{D16}h_{D16} \\ = \dot{m}_{D9}h_{D9} + \dot{m}_{D17}h_{D17} + \dot{m}_{D10}h_{D10} \end{aligned} \quad (67)$$

$$\text{Mass conservation } \dot{m}_{D2} + \dot{m}_{D16} = \dot{m}_{D10} + \dot{m}_{D17} \quad (68)$$

$$\text{Concentration balance } \dot{m}_{D2}X_{\text{sea}} + \dot{m}_{D16}X_{16} = \dot{m}_{D17}X_{17} \quad (69)$$

Fifth effect

$$\begin{aligned} \text{Energy conservation } \dot{m}_{D10}h_{D10} + \dot{m}_{D2}h_{D2} + \dot{m}_{D17}h_{D17} \\ = \dot{m}_{D11}h_{D11} + \dot{m}_{D18}h_{D18} + \dot{m}_{D12}h_{D12} \end{aligned} \quad (70)$$

$$\text{Mass conservation } \dot{m}_{D2} + \dot{m}_{D17} = \dot{m}_{D12} + \dot{m}_{D18} \quad (71)$$

$$\text{Concentration balance } \dot{m}_{D2}X_{\text{sea}} + \dot{m}_{D17}X_{17} = \dot{m}_{D18}X_{18} \quad (72)$$

Double-effect absorption chiller

Modeling of absorption chiller system components is governed by mass conservation and energy conservation for both LiBr and H₂O.

$$\left(\sum \dot{m}\right)_{\text{inlet}} - \left(\sum \dot{m}\right)_{\text{outlet}} = 0 \quad (73)$$

$$\left(\sum \dot{m}C\right)_{\text{inlet}} - \left(\sum \dot{m}C\right)_{\text{outlet}} = 0 \quad (74)$$

$$\left(\sum \dot{m}h\right)_{\text{inlet}} - \left(\sum \dot{m}h\right)_{\text{outlet}} = 0 \quad (75)$$

Initial cost

After being familiarized with the system and its components' characteristics, according to the performance parameters of each component, the conforming initial cost is provided as below (Table 2):

And the total initial cost is obtained by summation of all initial costs of components within the cycle's working condition.

Applied constants

The prominent design parameters of different components of the cycle are summarized in Table 3.

Also, for SPTC the geometrical and physical properties are represented in Table 4 and Fig. 2.

Data

Before optimization, a base design has been defined with assuming constant value for optimization investigation design parameters. For further investigation on the same cycles, reader can use the data of three parts of cycle separately, CHP, absorption chiller, and MED. All mentioning parts can be designed separately by the use of boundary states of them. Tables 5–7 show the design state data of CHP, absorption chiller, and MED.

Table 2 Initial cost equations of all components

Component	Cost equation	References
Compressor	$\text{cost}_{\text{comp}} = \frac{71.1\dot{m}_{\text{air}}}{0.92-\eta_{\text{comp}}} \text{Pr}_{\text{comp}} \log(\text{Pr}_{\text{comp}})$	[29]
SPTC	$\text{cost}_{\text{SPTC}} = 240A_{\text{collectors}}$	[30]
Combustion chamber	$\text{cost}_{\text{CC}} = \frac{46.08\dot{m}_{\text{air}}}{0.995-0.98} (1 + \exp(0.018(T_{\text{GT}} - 273) - 26.4))$	[30]
Gas turbine	$\text{cost}_{\text{GT}} = \frac{479.34\dot{m}_{\text{gas}}}{0.92-\eta_{\text{turb}}} \log(\text{Pr}_{\text{turb}}) (1 + \exp(0.036(T_{\text{GT}} - 273) - 54.4))$	[29]
Steam turbine	$\text{cost}_{\text{ST}} = 6000 \left(\frac{\dot{W}_{\text{ST}}}{10^3}\right)^{0.7}$	[30]
Condenser	$\text{cost}_{\text{cond}} = 1773\dot{m}_{\text{HP}}$	[30]
pump	$\text{cost}_{\text{pump}} = 705.48 \left(\frac{\dot{W}}{10^3}\right)^{0.7} \left(1 + \frac{2}{1-\eta_{\text{pump}}}\right)$	[25]
HRSG	$\text{cost}_{\text{HRSG}} = 6570 \left(\left(\frac{Q_{\text{LPeco}}}{10^3 \Delta T_{\text{LPeco}}}\right)^{0.8} + \left(\frac{Q_{\text{LPeva}}}{10^3 \Delta T_{\text{LPeva}}}\right)^{0.8} + \left(\frac{Q_{\text{HPeco}}}{10^3 \Delta T_{\text{HPeco}}}\right)^{0.8} + \left(\frac{Q_{\text{HPeva}}}{10^3 \Delta T_{\text{HPeva}}}\right)^{0.8} + \left(\frac{Q_{\text{HPvap}}}{10^3 \Delta T_{\text{HPvap}}}\right)^{0.8} \right) + 21276\dot{m}_{\text{steam}} + 1184.4\dot{m}_{\text{gas}}^{1.2}$	[30]
Chiller	$\text{cost}_{\text{CHILLER}} = 0.855Q_{\text{gen}}$	[31]
MED	$\text{cost}_{\text{evaMED}} = 250.26UA_{\text{evaMED}} \times 10^{-3}$	[32]

Table 3 Design parameter of the system component

Component	Parameter	Value	
SPTC	Sun temperature/K	5800	
	Ambient temperature/K	298	
	Number of columns	10	
	Tube length/m	12.27	
Combustion chamber	Pressure drop	2%	
	CHP plant	Air mass flow/kg/s	15
CHP plant	Compressor isentropic efficiency	0.85	
	Gas turbine isentropic efficiency	0.85	
	Pressure ratio of compressor	9.6	
	Pressure ratio of gas turbine	8.5	
	Pump isentropic efficiency	0.90	
	Steam turbine isentropic efficiency	0.85	
	Absorption chiller	Chilled water temperature/°C	7
		Cooling water temperature/°C	27
		Condensing temperature (state C1)/°C	35
		Evaporation temperature (state 2)/°C	4
Absorber outlet solution Temperature (state C4)/°C		35	
MED	Generator temperature/°C	130	
	Exhausted gas temperature/°C	105	
	Condenser temperature/°C	48	
	Final effect's salinity/ppm	70	
	Molar mass of salt/g mol ⁻¹	58.5	
	Minimum temperature difference at condenser/°C	3	

Table 4 SPTC constant variables

SPTC parameter		
$D_{co} = 121 \text{ mm}$	$\epsilon_r = 0.15$	$K_r = 1$
$D_{ci} = 115 \text{ mm}$	$\epsilon_c = 0.88$	
$D_{ro} = 70 \text{ mm}$	$G_b = 800 \text{ W m}^{-2}$	$\gamma = 0.93$
$D_{ri} = 66 \text{ mm}$	$\sigma = 5.67 \times 10^{-8}$	$\tau = 0.96$
$\rho_c = 0.94$	$K_{tube} = 16 \text{ W m}^{-1} \text{ K}^{-1}$	$\alpha = 0.9$
$W = 5.76 \text{ m}$	$K_{cover} = 1.4 \text{ W m}^{-1} \text{ K}^{-1}$	

Table 5 Temperature, mass flow rate, and pressure of each state point of the CHP system

State#	Temperature/K	Mass flow/kg s ⁻¹	Pressure/bar
1	298.10	15.00	1.00
2	610.30	15.00	1.00
3	835.40	15.00	1.00
4	1300.00	15.00	1.00
5	298.10	0.20	1.00
6	863.10	15.20	1.11
7	780.50	15.20	1.11
8	538.50	15.20	1.11
9	505.50	15.20	1.11
10	491.40	15.20	1.11
11	400.80	15.20	1.11
12	773.00	2.27	40.00
13	327.12	2.27	0.15
14	327.12	–	0.15
15	327.22	0.11	15.00
16	471.44	0.11	15.00
17	471.44	0.11	15.00
18	471.92	2.27	40.00
19	523.50	2.27	40.00
20	523.50	2.27	40.00
21	373.00	15.20	1.11

Results and discussion

The results of the parametric study for finding the most sensitive parameters on exergy efficiency and total cost rate are presented and discussed. Then, optimization of the system based on those parameters is revealed in this section.

Sensitivity analysis

At the first stage of optimization, several parameters were available for optimization, such as high pressure and low

Table 6 Temperature, mass flow rate, and pressure of each state point of the absorption chiller refrigeration system

State#	Temperature/K	Mass flow/kg s ⁻¹	Concentration/%
C1	308.00	0.15	–
C2	277.00	0.15	–
C3	277.00	0.15	–
C4	308.00	2.07	0.56
C5	307.98	2.07	0.56
C6	335.74	2.07	0.56
C7	0.00	2.07	0.56
C8	403.00	1.99	0.58
C9	392.06	1.99	0.58
C10	0.00	1.99	0.58
C11	403.00	0.08	–
C12	355.93	0.08	–
C13	308.95	0.08	–
C14	353.00	0.07	–
C15	353.00	1.92	0.60
C16	321.83	1.92	0.60
C17	321.84	1.92	0.60
C18	300.00	17.50	–
C19	305.00	17.50	–
C20	285.00	17.05	–
C21	280.00	17.05	–
C22	300.00	20.15	–
C23	305.00	20.15	–

pressure of HRSG, high- and low-pressure pinch point temperature difference, gas and steam turbine inlet temperature, condenser pressure, and the number of rows of SPTC. Since optimization is a time-consuming process and excess of decision variables may cause a significant increase in computational cost, a parametric study has been done to consider each parameter's sensitivity on the objective functions of optimization. Here, each of the mentioned parameters has been checked separately.

The HRSG considered in this integrated energy system has two pressure levels: one with a higher value for steam turbine and the other with a lower value for the MED. The values of these pressures have significant effects on

the steam turbine power generation and the MED fresh-water production. In addition, designing these systems in higher working pressure imposes excessive initial cost to the system. Figures 4 and 5 show the high-pressure and low-pressure effects on the total cost rate (Eq. 12) and the exergy efficiency of the system (Eq. 7).

An increase in the HRSG high pressure, while keeping other parameters constant, increases the inlet enthalpy of the steam turbine, which increases the rate of power generation. According to Eq. (7), an increase in these parameters increases the net power generated in the system, which increases the first term in the numerator of Eq. (7). Since other parameters in this equation do not vary, the overall exergy efficiency increases accordingly. On the other hand, an increase in the HRSG low pressure keeping other parameters constant increases the rate of exergy destruction in the MED system due to the increase of the pressure drop within the ejector, which, with reference to Eq. (7), decreases the overall exergy efficiency. On the other hand, as an increase in the working fluid pressure leads to an enlargement of the HRSG system, based on Eq. (12), the total cost rate increases in both cases.

Variation of high pressure from 30 to 50 bars causes increase in exergy efficiency from 36.1 to 36.7%. This 0.5% increase in exergy imposes about 2 \$ h⁻¹ total cost rate to cycle. Increment of exergy efficiency is due to extracting more exergy from exhaust gases in HRSG stage for steam turbine which has lower exergy destruction compared to MED. Increasing low pressure from 12 bars to 30 bars causes a very small decrease in exergy efficiency (about 0.04%).

Pinch point temperature is one of the most prominent design parameters of heat exchanger that has a considerable effect on exergy destruction and cost rate of this unit, which makes it necessary to study this parameter's effect on cycle [26]. As there are two vapor generators (drum) in HRSG, two pinch points can be set for the cycle: one for high-pressure drum (high-pressure pinch point) and the other for low-pressure drum (low-pressure pinch point). Figures 6 and 7 represent overall exergy efficiency and total cost rate variation due to low-pressure pinch point temperature and high-pressure pinch point temperature, respectively. As it is illustrated, a higher pinch point due to the increment of the unrecovered available energy causes higher exergy

Table 7 Temperature, mass flow rate and pressure of each state point of the MED system

State#	Temperature/K	Mass flow/ kg-s ⁻¹	Pressure/bar	X/PPM
D1	298.15	2.87	1.00	39
D2	318.15	0.65	1.00	39
D3	362.10	0.30	0.15	–
D4	325.93	0.30	0.14	–
D5	325.93	0.30	0.14	–
D6	324.73	0.29	0.13	–
D7	324.73	0.29	0.13	–
D8	323.54	0.28	0.13	–
D9	323.54	0.28	0.13	–
D10	322.34	0.28	0.12	–
D11	322.34	0.28	0.12	–
D12	321.15	0.28	0.11	–
D13	321.15	0.28	0.11	–
D14	325.93	0.35	–	71.79
D15	324.73	0.71	–	71.79
D16	323.54	1.07	–	70.96
D17	322.34	1.44	–	70.39
D18	321.15	1.81	–	70.00

destruction. Also, lower pinch point temperature necessitates better design for enhancement of the heat exchanger, which may increase the total cost rate. On the other side, as it declines the exergy destruction, it may lead to the reduction of the total cost rate.

Another critical parameter is the gas turbine inlet temperature, which has a significant effect on the whole cycle exergy efficiency since it defines the hot gas temperature flow in the HRSG. Figure 8 represents the variation of this parameter and its effect on overall exergy efficiency and the total cost rate. As the increment of the gas/steam turbine inlet temperature directly raises the conforming inlet enthalpy, which culminates in the growth rate of power generation, according to Eq. (7), the overall exergy efficiency is increased. Also, based on the conforming cost function of the gas/steam turbine, the total cost rate with respect to Eq. (12) is increased simultaneously. Higher gas turbine inlet temperature provides both higher exergy efficiency and better design considerations, which increases the total cost rate.

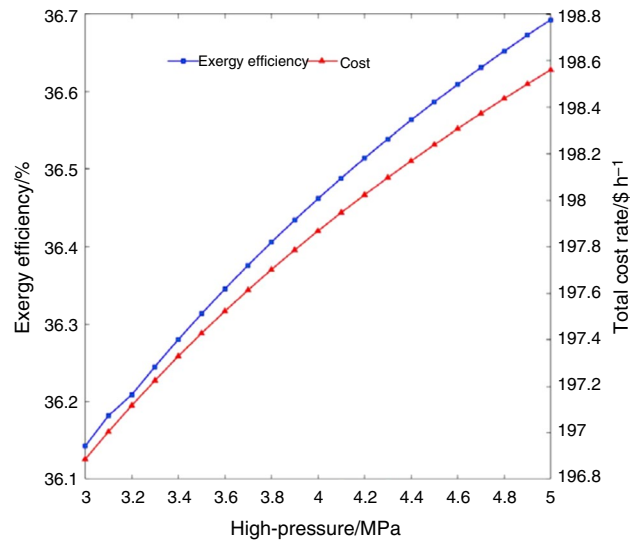


Fig. 4 Parametric study of high pressure of HRSG (inlet pressure of steam turbine)

Steam flow temperature at the inlet of steam turbine is another effective performance parameter. Figure 9 shows the variation of this parameter effect on exergy destruction and cost rate. As can be interpreted from the mentioned figure, the exergy efficiency increases because the variation of this parameter does not overcome the cost rate increase due to the design cost rate.

The next parameter is the condenser pressure, which affects the steam turbine and MED concurrently. The rise of the condenser pressure increases the steam turbine’s outlet enthalpy, decreasing the rate of power generation. According to Eq. (7), the overall exergy efficiency decreases as the decrease in net output power reduces the overall exergy efficiency of the system (see Eq. 7). A decrease in the condenser pressure downsizes several pieces of equipment including MED system, HRSG and steam turbine, but on the other side as the low-pressure pump of the HRSG would discharge a lower pressure which increases the flue gas outlet enthalpy, the generator heat of the absorption chiller goes up and accordingly enlarges the required chiller system and increases its initial cost. Figure 10 shows exergy efficiency and cost rate variation due to the variation of this parameter.

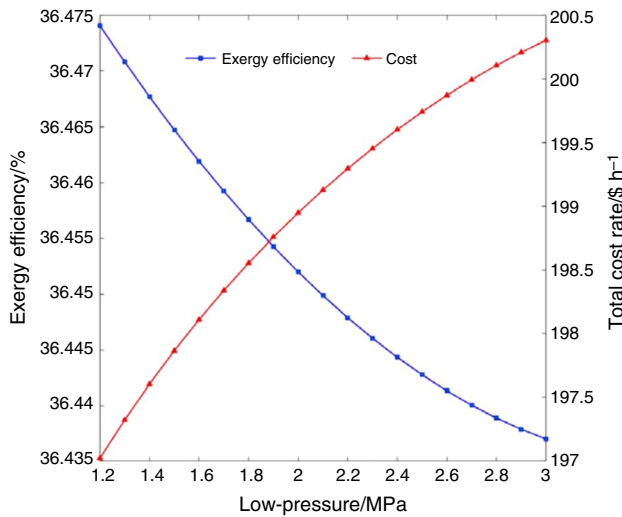


Fig. 5 Parametric study of low pressure of HRSG (inlet pressure of MED)

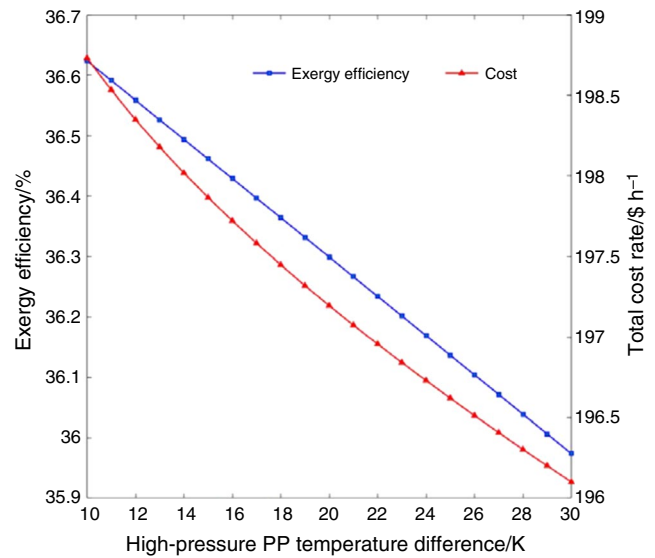


Fig. 7 Parametric study of high-pressure pinch point temperature

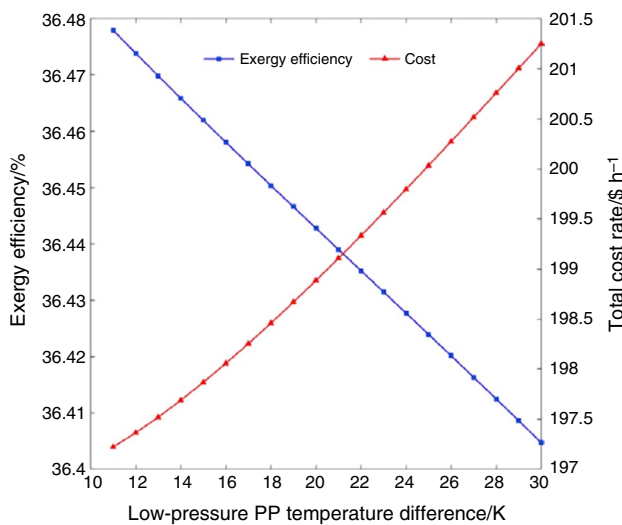


Fig. 6 Parametric study of low-pressure pinch point temperature

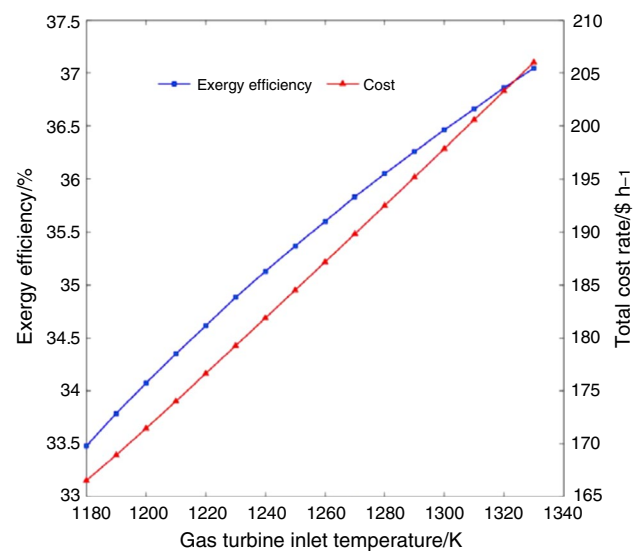


Fig. 8 Parametric study of gas turbine inlet temperature

Finally, row number of the SPTC is investigated as a parameter for the parametric study. According to Fig. 11, it can be inferred that as the number of SPTC rows raises, the surface area extends and the preheating temperature increases, which results in less fuel consumption and according to Eq. (12) leads to a lower total cost rate. Although

increase of the SPTC rows raises the input exergy to the cycle, the useful exergy obtained from the cycle remains constant, since other variable parameters' values are unchanged. Therefore, based on Eq. (7), overall exergy efficiency reduces.

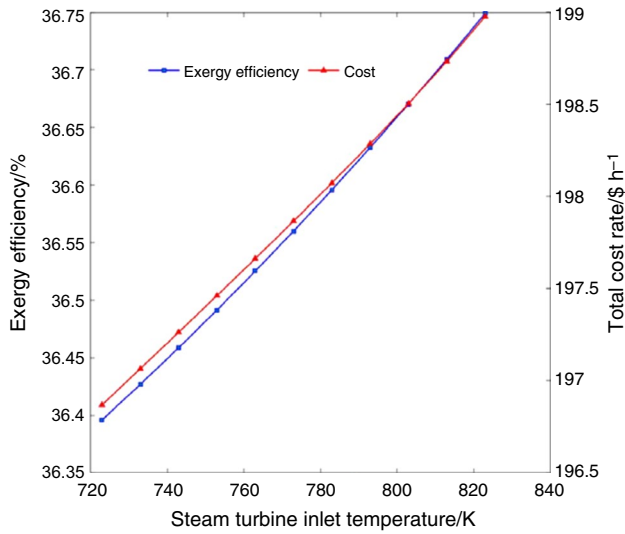


Fig. 9 Parametric study of steam turbine inlet temperature

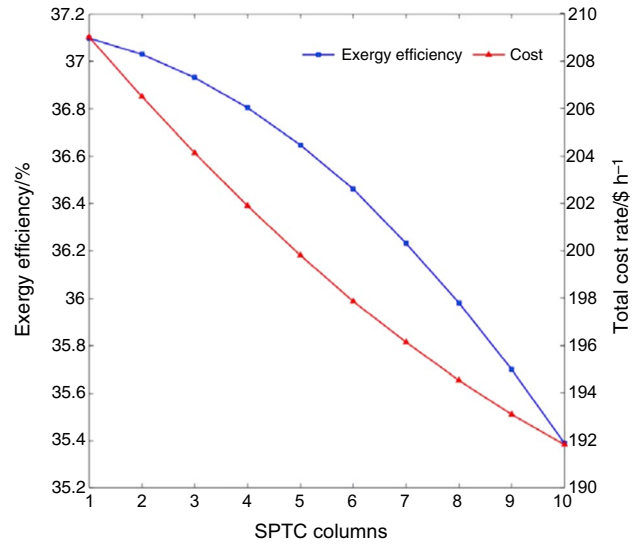


Fig. 11 Parametric study of number of SPTC rows

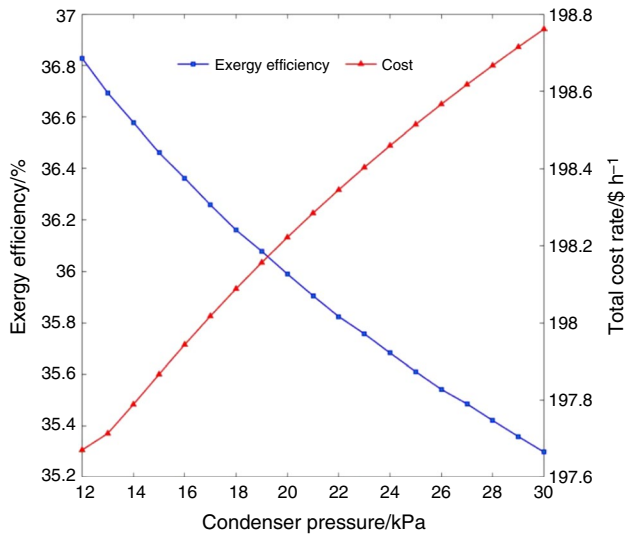


Fig. 10 Parametric study of condenser pressure

Optimization

Optimization is the best way to finalize a design [33]. Finally, using the genetic algorithm approach, an optimization procedure is accomplished; its objective functions have been chosen as the overall exergy efficiency and the total cost rate according to Eqs. (7) and (12), respectively. As

it could be deduced, the main objective is to maximize the overall exergy efficiency and simultaneously to minimize the total cost rate. Top six effective parameters including condenser pressure, number of SPTC rows, gas and steam turbine inlet temperature, and high- and low-pressure pinch points which have substantial effects on the objective functions as discussed in the previous section, have been chosen as decision variables.

Due to the existence of physical limitations including commercial availability or thermodynamic restrictions, applicable ranges of operation for each of these decision variables are defined in Table 8; also, these constraints are necessary for the performance of the genetic algorithm since they are set as the bonds of the search domain within which this evolutionary algorithm functions.

For better comparison, optimization has been done for three discount rates of $i = 0.11, 0.13, \text{ and } 0.15$. Pareto front results for these three discount rates are shown in Fig. 12. Optimization study has been accomplished using MATLAB genetic algorithm toolbox.

As could be understood from Fig. 12, the exergy efficiency has changed 8% in optimization study for the discount rate of 0.11 and also the total cost rate has changed up to 90 \$ h⁻¹, which represents a noticeable variation. It is worth noting that the higher ranges of changes were not observed at the parametric study, which reminds the effectiveness of optimization investigation.

Table 8 Constraints of optimization [26]

Parameter	Range	Reason
Gas turbine inlet temperature	$T_{GT} \leq 1550 \text{ }^\circ\text{C}$	Metrological limitation
Steam turbine inlet temperature	$T_{ST} \leq 550 \text{ }^\circ\text{C}$	Turbine inlet temperature limitation
Low-pressure pinch point	$PP_{LP} \leq 30 \text{ }^\circ\text{C}$	Heat transfer area limitation
High-pressure pinch point	$PP_{HP} \leq 30 \text{ }^\circ\text{C}$	Heat transfer area limitation
Condenser pressure	$P_{cond} \leq 30 \text{ Kpa}$	Net power limitation
Number of SPTC rows	$N_{row} \leq 10$	Commercial limitation

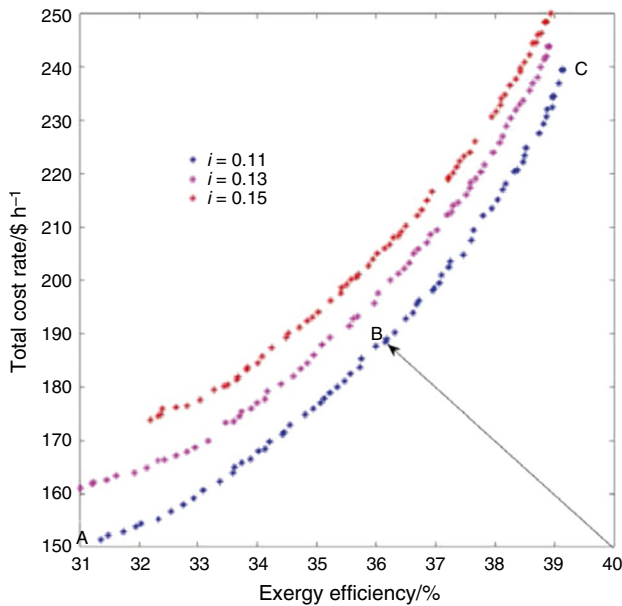


Fig. 12 Pareto front for three different discount rates

Three points named I, I, and I in Fig. 12 indicate three prominent design points, which are characterized as point A, the lowest total cost rate, point C the highest exergy efficiency, and a moderate design point at B, which is the

decision point since both exergy efficiency and total cost rate are in the intermediate level. Each point on the Pareto curve represents a set of decision variables. Since we have the index of the matrix for each point on the Pareto curve, it is easy to find their decision variables.

As can be seen in Fig. 12, for higher discount rates, Pareto front at a fixed exergy efficiency provides a higher total cost rate, and for a given total cost rate, lower discount rates provide higher exergy efficiency. The decision variables related to points A, B, and C are listed in Table 9, and the outputs related to these points are listed in Table 10. As it could be interpreted from Table 9 for higher exergy efficiency, a lower number of solar panel rows and condenser pressure and higher gas and steam turbine inlet temperature and pinch points are suggested by Pareto front results. Table 10 shows the final objective functions plus power and pure water generation and cooling load of the aforementioned points. Higher efficiency deals with a higher value of power generation as it is expected. The lower value of pure water generation is related to exergy destruction within the ejector. In the absorption chiller, there is a high-temperature difference in its different components like evaporator, condenser, and absorber, which causes high exergy destruction, so for higher exergy efficiency, it is better to have a lower value of the cooling load.

Table 9 Decision variables of Pareto front optimal point

Point	N_{column}	$P_{condenser}/\text{Kpa}$	$T_{gas\ turbine}/\text{K}$	$PP_{high\ pressure}/\text{K}$	$T_{steam\ turbine}/\text{K}$	$PP_{lo\ pressure}/\text{K}$
A	9	13.78	1150.1	13	725.8	12.1
B	5	12.53	1256	12.43	792	13.67
C	2	12.94	1408.8	16.45	809.4	26.9

Table 10 Objective functions and other results of Pareto front optimal point

State#	$E_{efficiency}$	Cost rate/\$ h ⁻¹	Power/MW	Cooling load/kW	Pure water/kg s ⁻¹
A	31.35	151.49	3.77	633.64	3.3258
B	36.16	188.43	5.18	406.18	2.5698
C	39.13	239.38	7.19	257.83	0.0744

Conclusions

An integrated CHP with water desalination system including solar Bryton cycle, HRSG, MED, and absorption chiller was investigated in this study economically and thermodynamically for various operating ranges of input parameters for each component of this integrated cycle. Variation of each parameter within its proposed range on the exergy efficiency and the total cost rate of the cycle was investigated while considering a fixed value for other parameters according to the base design states as listed in Tables 5–7. For example, changing the number of rows of the solar collectors from 1 to 10 decreased the overall exergy efficiency around 1.7% and the total cost rate by 17\$ h⁻¹. Variation of low-pressure pinch point from 10 to 30 K decreased overall exergy efficiency less than 0.8% and increased the total cost rate around 4 \$ h⁻¹, while in a similar case for high-pressure pinch, both the overall exergy efficiency and total cost rate decreased by more than 0.6 % and about 2.5 \$ h⁻¹, respectively. Alternation of gas turbine inlet temperature between 1180 K and around 1340 K yielded increase of exergy efficiency around 3.5% and total cost rate about 40 \$ h⁻¹, and variation of condenser pressure from 12 to 30 kpa decreased the exergy efficiency less than 1.6% and increased total cost rate about 1 \$ h⁻¹.

Most effective parameters were considered as the decision variables of a genetic algorithm with objective functions as the exergy efficiency and total cost rate, and the Pareto curve was obtained for various amounts of discount rates. Results revealed that higher condenser pressure yields higher exergy destruction while increasing the amount of freshwater generation; also, as the inlet temperature of turbines increases, both exergy efficiency and cost rate rise. Therefore, the optimal point could be chosen based on the proposed outcome of the cycle, including net electrical power, cooling load, and pure water generation. Pareto front curve results show that points with higher exergy efficiency have a lower number of solar collectors, lower pressure condenser, higher gas and steam turbine inlet temperature, and higher pinch points.

References

- Gao J, Kang J, Zhang C, Gang W. Energy performance and operation characteristics of distributed energy systems with district cooling systems in subtropical areas under different control strategies. *Energy*. 2018;153:849–60.
- Maleki A, Nazari MA, Pourfayaz F. Harmony search optimization for optimum sizing of hybrid solar schemes based on battery storage unit. *Energy Reports*. 2020.
- Maheshwari M, Singh O. Comparative evaluation of different combined cycle configurations having simple gas turbine, steam turbine and ammonia water turbine. *Energy*. 2019;168:1217–36.
- Kaplan PO, Witt JW. What is the role of distributed energy resources under scenarios of greenhouse gas reductions? A specific focus on combined heat and power systems in the industrial and commercial sectors. *Appl Energy*. 2019;235:83–94.
- Ameri M, Ahmadi P, Khanmohammadi S. Exergy analysis of a 420 MW combined cycle power plant. *Int J Energy Res*. 2008;32(2):175–83.
- Lake A, Rezaie B, Beyerlein S. Review of district heating and cooling systems for a sustainable future. *Renew Sustain Energy Rev*. 2017;67:417–25.
- Duffie JA, Beckman WA. *Solar engineering of thermal processes*. New York: Wiley; 2013.
- Arabkoohsar A, Sadi M. A solar PTC powered absorption chiller design for Co-supply of district heating and cooling systems in Denmark. *Energy*. 2019;193:116789.
- Shahdost BM, Jokar MA, Astarai FR, Ahmadi MH. Modeling and economic analysis of a parabolic trough solar collector used in order to preheat the process fluid of furnaces in a refinery (case study: Parsian Gas Refinery). *J Therm Anal Calorim*. 2019;137(6):2081–97.
- Arabkoohsar A, Sadi M. Thermodynamics, economic and environmental analyses of a hybrid waste–solar thermal power plant. *J Therm Anal Calorim*; 2020.
- Acar MS, Arslan O. Energy and exergy analysis of solar energy-integrated, geothermal energy-powered Organic Rankine Cycle. *J Therm Anal Calorim*. 2019;137(2):659–66.
- Islam SMF, Karim Z. *World's demand for food and water: the consequences of climate change. Desalination-challenges and opportunities*. London: IntechOpen; 2019.
- Hameed M, Moradkhani H, Ahmadalipour A, Moftakhari H, Abbaszadeh P, Alipour A. A review of the 21st century challenges in the food-energy-water security in the Middle East. *Water*. 2019;11(4):682.
- Velmurugan A, Swarnam P, Subramani T, Meena B, Kaledhonkar M. *Water demand and salinity. Desalination-challenges and opportunities*. London: IntechOpen; 2020.
- Razmi A, Soltani M, Tayefeh M, Torabi M, Dusseault M. Thermodynamic analysis of compressed air energy storage (CAES) hybridized with a multi-effect desalination (MED) system. *Energy Convers Manag*. 2019;199:112047.
- Moghimi M, Emadi M, Akbarpoor AM, Mollaei M. Energy and exergy investigation of a combined cooling, heating, power generation, and seawater desalination system. *Appl Therm Eng*. 2018;140:814–27.
- Farsi A, Dincer I. Development and evaluation of an integrated MED/membrane desalination system. *Desalination*. 2019;463:55–68.
- Vakilabadi MA, Bidi M, Najafi A, Ahmadi MH. Energy, exergy analysis and performance evaluation of a vacuum evaporator for solar thermal power plant Zero Liquid Discharge Systems. *J Therm Anal Calorim*. 2020;139(2):1275–90.
- Rostamzadeh H, Ghiasirad H, Amidpour M, Amidpour Y. Performance enhancement of a conventional multi-effect desalination (MED) system by heat pump cycles. *Desalination*. 2020;477:114261.
- Aguilar-Jiménez J, Velázquez N, López-Zavala R, Beltrán R, Hernández-Callejo L, González-Urbe L, et al. Low-temperature multiple-effect desalination/organic Rankine cycle system with a novel integration for fresh water and electrical energy production. *Desalination*. 2020;477:114269.
- Mahdavi N, Khalilarya S. Comprehensive thermodynamic investigation of three cogeneration systems including GT-HRSG/RORC

- as the base system, intermediate system and solar hybridized system. *Energy*. 2019;181:1252–72.
22. Wang J, Lu Z, Li M, Lior N, Li W. Energy, exergy, exergoeconomic and environmental (4E) analysis of a distributed generation solar-assisted CCHP (combined cooling, heating and power) gas turbine system. *Energy*. 2019;175:1246–58.
 23. Naseri A, Fazlikhani M, Sadeghzadeh M, Naeimi A, Bidi M, Tabatabaei SH. Thermodynamic and exergy analyses of a novel solar-powered CO₂ transcritical power cycle with recovery of cryogenic LNG using stirling engines. *Renew Energy Res Appl*. 2020;1(2):175–85.
 24. Jalili M, Cheraghi R, Reisi M, Ghasempour R. Energy and exergy assessment of a new heat recovery method in a cement factory. *Renew Energy Res Appl*. 2020;1(1):123–34.
 25. Dincer I, Rosen MA, Ahmadi P. Optimization of energy systems. New York: Wiley; 2017.
 26. Ahmadi P, Dincer I. Thermodynamic analysis and thermoeconomic optimization of a dual pressure combined cycle power plant with a supplementary firing unit. *Energy Convers Manag*. 2011;52(5):2296–308.
 27. Mirzaei M, Ahmadi MH, Mobin M, Nazari MA, Alayi R. Energy, exergy and economics analysis of an ORC working with several fluids and utilizes smelting furnace gases as heat source. *Therm Sci Eng Progress*. 2018;5:230–7.
 28. Ettouney HEDH. Single-effect thermal vapor-compression desalination process: thermal analysis. *Heat Transf Eng*. 1999;20(2):52–68.
 29. Gholamian E, Hanafizadeh P, Habibollahzade A, Ahmadi P. Evolutionary based multi-criteria optimization of an integrated energy system with SOFC, gas turbine, and hydrogen production via electrolysis. *Int J Hydrog Energy*. 2018;43(33):16201–14.
 30. Habibollahzade A, Gholamian E, Ahmadi P, Behzadi A. Multi-criteria optimization of an integrated energy system with thermoelectric generator, parabolic trough solar collector and electrolysis for hydrogen production. *Int J Hydrog Energy*. 2018;43(31):14140–57.
 31. Shirazi A, Taylor RA, Morrison GL, White SD. A comprehensive, multi-objective optimization of solar-powered absorption chiller systems for air-conditioning applications. *Energy Convers Manag*. 2017;132:281–306.
 32. Hafdhi F, Khir T, Yahia AB, Brahim AB. Exergoeconomic optimization of a double effect desalination unit used in an industrial steam power plant. *Desalination*. 2018;438:63–82.
 33. Pakatchian MR, Saeidi H, Ziamolki A. CFD-based blade shape optimization of MGT-70 (3) axial flow compressor. *Int J Numer Methods Heat Fluid Flow*; 2019.

Publisher's Note Springer Nature remains neutral with regard to jurisdictional claims in published maps and institutional affiliations.